American Mineralogist, Volume 92, pages 139–150, 2007

Reversed phase equilibrium constraints on the stability of Mg-Fe-Al biotite

R.G. BERMAN,[1,*] L. YA. ARANOVICH,[2] D.G. RANCOURT,[3] AND P.H.J. MERCIER[4]

[1]Geological Survey of Canada, 615 Booth Street, Ottawa, Ontario, Canada K1A 0E9
[2]Institute of Geology of Ore Deposits, Petrography, Mineralogy, and Geochemisty, 119017 Moscow, Russia
[3]Department of Physics, University of Ottawa, Ottawa, Ontario, Canada K1N 6N5
[4]Institute for Chemical Process and Environmental Technology, National Research Council Canada, 1200 Montreal Road, Ottawa, Ontario, Canada K1A 0R6

ABSTRACT

The stability of Mg-Fe-Al biotite has been investigated with reversed phase-equilibrium experiments on four equilibria. Experimental brackets in pure H_2O and H_2O-CO_2 mixtures for the equilibrium:

phlogopite + 3 quartz = enstatite + sanidine + H_2O (1)

are in good agreement with previous experiments in mixed-volatile fluids (Bohlen et al. 1983) and H_2O-KCl solutions (Aranovich and Newton 1998), while indicating a reduced stability field for phlogopite compared to previous data in pure H_2O (Wood 1976; Peterson and Newton 1989). Aluminum solubility in biotite has been determined in the Fe-, Mg-, and Fe-Mg systems from reversed phase-equilibrium data for the equilibria:

3 eastonite + 6 quartz = 2 phlogopite + 3 sillimanite + sanidine + H_2O (2)

3 siderophyllite + 6 quartz = 2 annite + 3 sillimanite + sanidine + H_2O (3)

over the *P-T* range ~600–750 °C and 1.1–3.4 kbar. Over the investigated temperatures, the brackets define nominal Al saturation levels of 1.60 ± 0.04 in Mg-biotite, 2.08 ± 0.05 in Fe-biotite, and 1.81 ± 0.03 in biotite with Fe/(Fe + Mg) = 0.43–0.44. The slight decrease in Al with increasing *T* and decreasing *P* suggested by the data is less than experimental uncertainties.

Compared to biotite on the Phl–Ann join, Al-saturated biotites have a markedly larger stability field, particularly in the Fe-system. This effect has been quantified in the Fe-system with one reversal between 691–709 °C at 2.4 kbar for the equilibrium:

biotite + sillimanite + quartz = almandine + sanidine + H_2O (4)

The combined experimental results place tight constraints on the thermodynamic properties of phlogopite, annite, eastonite, and siderophyllite. The resulting nonzero (ΔH_{298} = –9.4 kJ/mol, with $\Delta S = \Delta V = 0$) energetics for the internal equilibrium:

Eastonite + 2/3 Annite = 2/3 Phlogopite + Siderophyllite (5)

reflect strong Fe-Al affinity in biotite, which has a marked effect on thermobarometers involving biotite.

Keywords: Biotite, phase equilibria, experimental petrology, mixing properties, annite, phlogopite, siderophyllite, eastonite

INTRODUCTION

Biotite is a particularly important mineral in metamorphic rocks because of its occurrence not only in nature over a wide range of bulk compositions and metamorphic grades, but also computationally in numerous equilibria that represent useful thermobarometers and boundaries on petrogenetic grids. In spite of its obvious importance, quantitative calculations involving biotite continue to be relatively uncertain, as evidenced by major differences in computed petrogenetic grids for metapelites (e.g., Spear and Cheney 1989; Powell and Holland 1990; Pattison and Tracy 1991; Xu et al. 1994) and thermobarometric formulations involving biotite (e.g., Ferry and Spear 1978; Perchuk and Lavrent'eva 1983; Aranovich et al. 1988; Holdaway et al. 1997).

* E-mail: RBerman@NRCan.gc.ca

0003-004X/07/0001–139$05.00/DOI: 10.2138/am.2007.2051

Much of this uncertainty stems from incomplete knowledge of the stability of the most important biotite end-members, phlogopite and annite. In the Mg-system, phase-equilibrium results on the stability field of phlogopite + quartz relative to enstatite + K-feldspar in pure H_2O (Wood 1976; Wones and Dodge 1977; Peterson and Newton 1989; Clemens 1995) are compatible with one another. However, all are discordant with experimental results that require a smaller stability field for phlogopite in mixed H_2O-CO_2 (Bohlen et al. 1983) and H_2O-KCl (Aranovich and Newton 1998) fluids. Calorimetric measurements of Circone and Navrotsky (1992) yielded an even smaller stability field for phlogopite. Annite (±quartz) stability has been studied by Dachs (1994) and Cygan et al. (1996) using different modifications of hydrogen sensor techniques and by Dachs and Benisek (1995) with the conventional oxygen buffer quartz-fayalite-magnetite (QFM). These experimental results yield thermodynamic properties for annite that differ by approximately 15 kJ/mol.

Even more severe uncertainties attend calculations involving the aluminous biotite end-members, eastonite and siderophyllite. Circone and Navrotsky (1992) determined the enthalpy of formation of eastonite by solution calorimetry, but associated uncertainties are large. Rutherford (1973) and Robert (1976) performed phase-equilibrium experiments involving siderophyllite and eastonite, respectively. Although of limited use for quantitative modeling due to the unreversed nature of these experiments, these data illustrate the important effect that excess Al has in expanding the thermal stability of biotite, an effect that explains some differences between petrogenetic grids computed with excess Al in biotite (e.g., Powell and Holland 1990; Xu et al. 1994) and without excess Al in biotite (Spear and Cheney 1989).

The present contribution is aimed at resolving some of the deficiencies and discrepancies cited above. Phlogopite stability is assessed with reversed phase-equilibrium data in both mixed H_2O-CO_2 and pure H_2O fluids for the equilibrium (see Table 1 and Kretz 1983 for abbreviations):

$$\text{Phl} + 3\ \text{Qtz} = 3\ \text{En} + \text{Sa} + \text{H}_2\text{O} \quad (1)$$

The stabilities of eastonite, siderophyllite, and annite are evaluated with reversals of the equilibria:

$$3\ \text{Eas} + 6\ \text{Qtz} = 2\ \text{Phl} + 3\ \text{Sil} + \text{Sa} + \text{H}_2\text{O} \quad (2)$$

$$3\ \text{Sdr} + 6\ \text{Qtz} = 2\ \text{Ann} + 3\ \text{Sil} + \text{Sa} + \text{H}_2\text{O} \quad (3)$$

$$\text{Sdr}_{55} + \text{Sil} + \text{Qtz} = \text{Alm} + \text{Sa} + \text{H}_2\text{O} \quad (4)$$

These experiments constrain thermodynamic data for the above end-members, with attendant improvements in quantitative calculations involving biotite. Preliminary results of this study were presented by Berman et al. (1995a, 1995b).

Experimental methods

Hydrothermal apparatus

Experiments, performed at the Geological Survey of Canada in Ottawa, were conducted in cold-seal hydrothermal apparati, with pressure vessels made from Haynes Alloy no. 25 (stellite) or René 41. The pressure medium was either H_2O (for Mg-system runs) or CH_4 (for Fe-system runs). Each pressure vessel was monitored by a 60 000 psi digital strain sensor (±0.2% linearity), calibrated to a Heise burdon-tube gauge certified by the manufacturer as accurate to ±0.1% of full scale (0–50 000 psi). The Heise gauge was maintained at 1 atm except when calibrating the transducers. Reported pressures are believed to be accurate to within ±15 bars.

Temperatures were controlled and monitored continuously by a digital data acquisition and control system made by Scimetric Inc., Ottawa, Ontario. Temperatures were measured using chromel-alumel thermocouples sheathed in inconel, inserted into a 2 cm well adjacent to the experimental charge. Each thermocouple was calibrated periodically against a lab standard to check for thermocouple drift with extended use. The lab standard was calibrated against the melting points of Zn (440.3 °C), Al (660.8 °C), and Ag (860 °C). Offsets of measuring thermocouples relative to a "standard" thermocouple placed within the pressure vessels were <5 °C at 1 atmosphere. Measurements at 1 atm indicate that temperature gradients were between 1.5 and 3 °C over a distance of 3.0 cm. Temperature uncertainties reported in Tables 2–4 represent the sum of uncertainties due to fluctuations over the duration of the experiment, thermocouple calibration uncertainties (1 °C), temperature gradients over the length of run capsules, and the temperature gradient across the Scimetric control unit in which the zero point emf correction is made (1 °C).

Several experiments on Equilibrium 1 were also performed at the University of Chicago, in an internally heated argon-pressure vessel. Details of the pressure and temperature control in this apparatus are given in (Goldsmith and Jenkins 1985). Uncertainties in the *P-T* measurements are estimated ±3 °C and 50 bars, respectively.

Experimental procedures

Experiments with H_2O-CO_2 fluid used 3 mm O.D. (0.1 mm wall) Au or 3.5 mm O.D. (0.2 mm wall) Pt capsules, containing about 5 mg of either $Ag_2C_2O_4$ +

Table 1. Unit-cell parameters and Fe^{3+} contents of synthetic starting materials

Name	Abbrev	Formula	*a* (Å)	*b* (Å)	*c* (Å)	β (°)	*V* (Å^3)	Fe^{3+}_{tet}	Fe^{3+}_{oct}
Annite*	Ann	$K(Fe_3)(AlSi_3)O_{10}(OH)_2$	5.404(5)	9.359(5)	10.327(5)	100.051(37)	514.36(32)	6.57(17)	3.08(20)
$Siderophyllite_{80}$	Sdr_{80}	$K(Fe_{2.2}Al_{0.8})(Al_{1.8}Si_{2.2})O_{10}(OH)_2$	5.374(6)	9.267(4)	10.260(3)	100.120(26)	503.03(40)		
$Siderophyllite_{55}$*	Sdr_{55}	$K(Fe_{2.45}Al_{0.55})(Al_{1.55}Si_{2.45})O_{10}(OH)_2$	5.372(8)	9.307(5)	10.264(7)	100.050(72)	505.34(33)	bdl	5.26(35)
$Ann_{50}Phl_{50}$*	FM_{50}	$K(Fe_{1.5}Mg_{1.5})(AlSi_3)O_{10}(OH)_2$	5.360(6)	9.283(5)	10.317(7)	99.977(31)	505.52(37)	5.08(41)	2.23(49)
$Sdr_{80}FM_{50}$*	$Sdr_{80/50}$	$K(Fe_{1.1}Mg_{1.1}Al_{0.8})(Al_{1.8}Si_{2.2})O_{10}(OH)_2$	5.322(7)	9.217(5)	10.275(6)	99.943(34)	496.43(40)	bdl	4.85(24)
Almandine	Alm	$Fe_3Al_2Si_3O_{12}$	11.533(1)				1534.16(38)	nd	
Enstatite	En	$MgSiO_3$	18.197(4)	8.803(2)	5.166(1)		827.48(24)		
Phlogopite	Phl	$K(Mg_3)(AlSi_3)O_{10}(OH)_2$	5.305(1)	9.202(2)	10.295(3)	99.867(18)	495.07(14)		
$Eastonite_{55}$	Eas_{55}	$K(Mg_{2.45}Al_{0.55})(Al_{1.55}Si_{2.55})O_{10}(OH)_2$	5.297(1)	9.165(2)	10.295(3)	99.914(25)	492.32(18)		
Sanidine	Sa	$KAlSi_3O_8$	8.605(8)	13.021(4)	7.183(4)	116.01(27)	723.31(19)		

Notes: Cell refinements were indexed 17–18 peaks except as noted below. bdl = below detection level; nd = not determined.
* Samples described by Mercier et al. (2005) were indexed on 33–35 peaks.

TABLE 2. Experiments on Equilibrium 1: Phl + 3 Qtz = 3 En + Sa + H_2O

Run no.	Time (days)	T (°C)	P (kbar)	X_{CO_2} (initial)	X_{CO_2} (final)	Stable Assemblage	% Reaction Observed
2	25	780±5.0	2.56±0.08	0.79	nd	En + Sa	100
3	18	782±6.0	2.49±0.05	0.67	0.65	En + Sa	100
5	23	772±4.0	2.53±0.06	0.35	0.38	Phl + Qtz	90
8	22	696±6.0	2.54±0.04	0.5	0.51	Phl + Qtz	100
10	22	756±5.0	2.47±0.03	0.5	0.47	Phl + Qtz	90
11	22	810±6.0	2.49±0.08	0.5	0.47	?	0
12	22	771±7.0	2.61±0.09	0.5	0.39	Phl + Qtz	100
14	21	757±7.0	1.76±0.02	0.45	0.45	Phl + Qtz	30
15	18	782±6.5	1.74±0.03	0.45	0.45	En + Sa	70
18	21	768±4.0	1.74±0.02	0.45	0.49	En + Sa	40
19	21	760±4.0	1.74±0.02	0.45	0.49	Phl + Qtz	50
20	23	769±5.0	0.46±0.025	0	0	En + Sa	60
22	23	755±5.0	0.49±0.025	0	0	Phl + Qtz	70
PQ1	18	765±3.0	2.00±0.05	0.5	0.5	Phl + Qtz	70
PQ2	14	770±3.0	2.00±0.05	0.5	0.49	No reaction	
PQ3	11	780±3.0	2.00±0.05	0.5	0.51	En + Sa	70

Note: All fluid compositions represent initial compositions based on weighed amounts of $Ag_2C_2O_4$ + H_2O, except for runs no. 14–19 and PQ, in which oxalic acid was used, and no. 20–22, which used pure H_2O; *P-T* uncertainties represent the sum of both precision and accuracy.

TABLE 3. Al saturation data for the assemblage biotite-Sil-Sa-Qtz-H_2O

Run no.	Duration (Days)	T (°C)	P (kbar)	X_{Fe}	Initial Al	Final Al	No. grains—avg*
E23	24	700±4	1.24±0.07	0.0	1.0	1.38–1.63	20-3
E24	24	700±4	1.24±0.07	0.0	2.1	1.77–1.58	11-3
E25	24	647±4	1.12±0.03	0.0	1.0	1.24–1.59	21-2
E26	24	647±4	1.12±0.03	0.0	2.1	1.96–1.64	22-3
E30	17	755±4	1.12±0.03	0.0	1.0	1.30–1.56	11-2
E29	17	755±4	1.12±0.03	0.0	2.1	1.74–1.61	10-3
E21	29	702±4	3.20±0.05	0.0	1.0	1.35–1.64	12-2
E22	29	702±4	3.20±0.05	0.0	2.1	1.82–1.64	17-3
S1	24	699±5	1.97±0.09	1.0	1.0	1.88–2.08	13-3
S2	24	699±5	1.97±0.09	1.0	2.6	2.31–2.03	12-2
S3	28	647±4	2.05±0.03	1.0	1.0	1.87–2.06	14-2
S4	28	647±4	2.05±0.03	1.0	2.6	2.51–2.08	16-3
S5†	20	777±5	2.03±0.07	1.0	2.6		
S6†	20	777±5	2.03±0.07	1.0	1.0		
S8	47	606±4	2.06±0.06	1.0	1.0	1.92–2.08	11-2
S7	47	606±4	2.06±0.06	1.0	2.6	2.41–2.13	13-2
S9	21	698±5	3.51±0.13	1.0	1.0	1.42–2.13	13-3
S10	21	698±5	3.51±0.13	1.0	2.6	2.38–2.12	12-2
A32	36	709±8	2.06±0.06	0.43	1.0	1.43–1.78	13-3
A31	36	709±8	2.06±0.06	0.44	2.6	1.98–1.83	14-3

Notes: Al values = no. of Al cations based on 22 negative charge formula; X_{Fe} = final Fe/(Fe + Mg).
* No. of grains analyzed—no. of grains averaged for most advanced composition (see text).
† Bt replaced by Alm + Sil + Qtz + hercynite + melt.

H_2O (carefully weighed to yield specific fluid compositions) or oxalic acid (for fluid compositions of X_{CO_2} = 0.49), together with about 5 mg of mineral mix A. This mix contained about 10 wt% of the low-temperature assemblage of Equilibrium 1 (with molar proportions Phl:Qtz = 1:3) and 90% of the high-temperature assemblage (with molar proportions En:Sa = 3:1), homogenized by light grinding for about 10 minutes in an agate mortar. Experiments in the gas vessel were done in double capsules: an inner Pt capsule containing 5 mg of the starting mineral mix A and about 3 mg oxalic acid was welded shut and put in the outer Au capsule containing about 40 mg Fe_2O_3 and 5 mg H_2O, to prevent any possible reduction of the H_2O-CO_2 fluid during the runs. Experiments on Equilibrium 1 in pure H_2O used 2 mm O.D. (0.1 mm wall) Au capsules containing about 5 mg H_2O and 5 mg of mineral mix A.

To study Equilibria 2 and 3, two capsules were used in each experiment, one with low-Al biotite (Phl or Ann) and the other with high-Al biotite (Eas_{55} or Sdr_{80}), both mixed in subequal weight proportions with Sil, Sa, and Qtz. Each capsule contained about 5 mg of mix and 5 mg of H_2O. Experiments on Equilibrium 4 used about 5 mg of H_2O together with 5 mg of subequal proportions of products and reactants (the biotite used was Sdr_{55} described below). For all Fe-biotite syntheses and for Equilibria 3 and 4, hydrogen fugacity was controlled using the C-CH_4 buffer (Eugster and Skippen 1967), but no attempt was made to ascertain the attained fugacity values, which depend on the rate of H_2 diffusion out of the pressure vessels (Chou 1987; Chou and Cygan 1990). However, both unit-cell parameters and Fe^{3+} contents of the synthetic annite and Fe-Al biotite of this study (see below) correspond to those of the most reduced biotites reported in the literature (Hewitt and Wones 1975; Partin 1984; Rebbert et al. 1995; Benisek et al. 1996), indicating that reducing conditions were maintained during the experiments.

TABLE 4. Experiments on Equilibrium 4

No.	Duration (days)	T (°C)	P (kbar)	Stable Assemblage	% Reaction Observed
1	20	691±4.0	2.45±0.05	Bi + Sil + Qtz	70
3	24	709±4.0	2.34±0.09	Alm + Sa	30
4	23	728±5.0	2.48±0.07	Alm + Sa	70
2	21	748±4.0	2.43±0.07	Alm + Sa	90

The minerals used in the above mixes are described below. In all experiments, capsules were placed within a cavity in the end of a steel filler rod. The opposite (cold) end of the filler rod was tapped and threaded to facilitate its removal with the sample capsules at the conclusion of each experiment. Experiments were held at elevated pressure and temperature for durations of 18–29 days, monitored daily, and, for C-CH_4 experiments, the pressure was increased periodically to compensate for H_2 leakage out of the pressure vessel (Chou 1987). Experiments were quenched in a jet of compressed air to less than 100 °C within 3 minutes. Samples were examined optically, by XRD, SEM, and electron microprobe. For Equilibria 1 and 4, reversals were obtained by comparison of the intensities of non-overlapping XRD peaks (001 for the biotites; 610 for En; $\bar{1}30$ for Sa; 400 for Alm) of the run product with the starting material. A half-bracket was considered successful if more than 30% change in peak ratios was observed. Fluid compositions determined after each experiment could not be used as reliable monitors of reaction direction because the observed changes were of the same magnitude as the analytical uncertainties (see below). For Equilibria 2 and 3, reversals were obtained from electron-microprobe analysis of biotite compositions in run products. Successful runs produced biotite with similar Al contents from starting mixes that contained both low-Al and high-Al biotite.

Analytical methods

Powder X-ray diffraction patterns were collected over the 2θ range 5 to 90° with a Phillips X'Pert PW3710 automated powder diffractometer, using a step size of 0.01° 2θ and Cu$K\alpha$ radiation (45 kV/40 mA). Si metal (a = 5.43054 Å) was used as an internal standard in each run. Cell refinements were calculated with the LSURI computer program (Appleman and Evans 1973).

Fluid compositions of the run products of experiments on Equilibrium 1 were determined by the method of Johannes (1969). CO_2 was first determined by the weight lost upon puncturing sample capsules. H_2O was then determined by the additional weight lost after drying of the capsule at 120 °C. To minimize the escape of H_2O along with CO_2, capsules were either centrifuged prior to puncture (GSC experiments) or punctured frozen in liquid nitrogen (University of Chicago experiments). Blank experiments, performed to check for absorbed H_2O or breakdown of the silver oxalate through exposure to light, indicate reproducibility in determining fluid compositions near X_{CO_2} = 0.5 of about ±2 mol%. Blank experiments with oxalic acid buffered with hematite-magnetite (HM) reproduced the theoretical value of X_{CO_2} = 0.49 ± 0.01, i.e., within the uncertainties of the semi-analytical balance.

For SEM and microprobe analysis, samples were disaggregated by very light grinding in ethyl alcohol, finely dispersed by pipette on a polished graphite disc, and carbon coated. Biotite analyses (MgO, FeO, Al_2O_3, SiO_2, and K_2O) were collected on a CAMECA SX-50 electron microprobe operated at 15 keV and 10 nA sample current (2–3 μm spot size) in wavelength-dispersive mode. Standards used were near end-member natural minerals. Although oxide analytical totals of thin biotite flakes are commonly less than ideal (see results section), a strong advantage of analysis of dispersed biotite flakes, as opposed to pressed aggregated grains, is that it avoids mixed analytical results stemming from excitation of underlying or adjacent phases. Structural formulae were calculated on a fixed charge (–22) basis.

Mossbauer data were collected at the Department of Physics, Ottawa University, employing the techniques described by Rancourt et al. (2001).

RESULTS

Synthesis and characterization of starting materials

Phl and Eas_{55} [$K(Mg_{2.45}Al_{0.55})(Al_{1.55}Si_{2.45})$ $O_{10}(OH)_2$] were synthesized from stoichiometric mixtures of MgO, γ-Al_2O_3, K_2CO_3, and cristobalite. γ-Al_2O_3 and cristobalite were prepared by firing $Al(OH)_3$ and silicic acid, respectively, at 1000 °C for 20

hours. The MgO was also heated at 1000 °C for 20 hours to dry it completely. Annite was synthesized from stoichiometric mixtures of $KSi_3O_{6.5}$ glass, prepared by the method of Schairer and Bowen (1955), with iron oxalate ($FeC_2O_4 \cdot 2H_2O$), and γ-Al_2O_3. Fe-Mg-Al biotites were synthesized from iron oxalate, MgO, γ-Al_2O_3, K_2CO_3, and cristobalite, mixed to give the compositions Sdr_{80} [$K(Fe_{2.2}Al_{0.8})(Al_{1.8}Si_{2.2})O_{10}(OH)_2$], Sdr_{55} [$K(Fe_{2.45}Al_{0.55})(Al_{1.55}Si_{2.45})O_{10}(OH)_2$], $Sdr_{80}FM_{50}$ [$K(Mg_{1.1}Fe_{1.1}Al_{0.8})(Al_{1.8}Si_{2.2})O_{10}(OH)_2$], and FM_{50} [$K(Mg_{1.5}Fe_{1.5})(AlSi_3)O_{10}(OH)_2$]. Between 120 to 150 mg of each mixture was sealed in 4 mm O.D.-3.8 mm I.D. Au capsules and held for 7–13 days at 2 kbar and either 750 °C (Phl), 700 °C (Ann, FM_{50}), or 650 °C (Eas_{55}, Sdr_{80}, Sdr_{55}, and $Sdr_{80}FM_{50}$).

Powder XRD patterns, as well as optical and SEM examination indicated close to complete reaction of the Mg-bearing starting materials, with <1% corundum in the Eas_{55} synthesis. Microprobe analysis was hindered by the extremely fine-grained nature of the synthetic materials (1–5 µm; Fig. 1a), but showed no significant deviation from the expected stoichiometry. Analyses of the Eas_{55} material ranged from 2.02–2.12 total Al pfu, compared to the expected 2.10 Al pfu. Unit-cell parameters for phlogopite and Eas_{55} (Table 1) are similar to those obtained in other studies of phlogopite (Hewitt and Wones 1975; Bohlen et al. 1983; Peterson and Newton 1989) and Mg-Al biotite (Fig. 2; Hewitt and Wones 1975; Circone et al. 1991).

Minor amounts of fayalite and magnetite were discernible in XRD scans of Ann, which had a grain size between 2 and 20 µm. Similar impurities were reported in annite syntheses of Hewitt and Wones (1975), Partin (1984), Rebbert et al. (1995), and Dachs (1994). Syntheses of Fe-Mg-Al biotites, Sdr_{80}, Sdr_{55}, and $Sdr_{80}FM_{50}$ produced 1–10 µm biotite grains (e.g., Fig. 1b) with several corundum grains as the only detectable (by SEM) impurities. Microprobe analyses of the Sdr_{80} and Sdr_{55} synthesis products range between 2.44–2.56 and 2.04–2.12 total Al pfu (–22 charge basis), respectively. Mössbauer analysis of the synthetic starting materials shows marked reduction in tetrahedral Fe^{3+} in the aluminous biotites (below detection levels) vs. annite (6.6%). Aluminous biotites contain ~5% octahedral Fe^{3+}. These data are similar to wet-chemical and Mössbauer data of other synthetic annites and Fe-Al biotites (Partin 1984; Rebbert et al. 1995; Benisek et al. 1996).

Unit-cell parameters of most Fe-biotites used in this study (Table 1) were reported by Mercier et al. (2005) on the basis of 33–35 reflections. Previous experimental work (Rutherford 1973; Hewitt and Wones 1975; Partin 1984; Rebbert et al. 1995; Benisek et al. 1996) has shown that the molar volume decreases with both increasing Al and increasing Fe^{3+} in biotite (Fig. 3). Our results are in excellent agreement with volumes determined from the most reduced biotites studied previously (Fig. 3), consistent with the Mossbauer measurements described above.

Enstatite was synthesized from stoichiometric mixtures of MgO and cristobalite, prepared as described above. Complete reaction of starting mixtures was obtained in experiments at 2 kbar and 800 °C for 3 days. Almandine was crystallized at 900 °C and 13 kbar from glass (see details of the synthesis procedure in Aranovich and Berman 1997). Comparison with Mossbauer and cell-edge data of Woodland and Wood (1989) suggests ~4% Fe^{3+} in the synthetic almandine. Sanidine was synthesized from

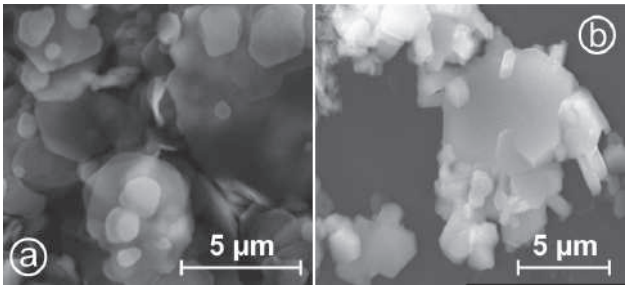

FIGURE 1. Secondary electron images showing the range of crystal size and morphology of synthetic biotite in starting materials: (**a**) $eastonite_{55}$; (**b**) $siderophillite_{80}$.

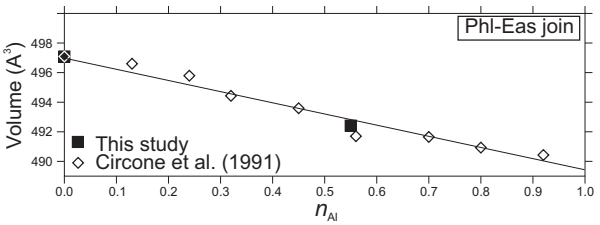

FIGURE 2. Variation of molar volume with n_{Al} (= ^{IV}Al-1 = ^{VI}Al) in Mg-Al-biotite.

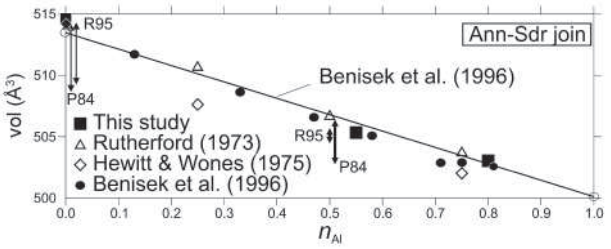

FIGURE 3. Variation of molar volumes with n_{Al} (= ^{IV}Al-1 = ^{VI}Al) in Fe-biotite. Paired arrows show range of volumes measured at different hydrogen pressures (see text) by Partin (1984; P84) and Rebbert et al. (1995; R95).

a stoichiometric mixture of K_2CO_3, $Al(OH)_3$, and cristobalite, reacted hydrothermally at 775 °C and 1 kbar for 3 days. Measurement of the (060)-($\bar{1}$13) peak-position difference (Hovis 1989) indicated that the synthesis product was approximately 12% ordered. Natural quartz (Lisbon) and sillimanite (Brandywine) were used in all experiments.

Experimental data for Equilibrium 1

Experimentally determined half-brackets are listed in Table 2, and plotted in Figures 4 and 5. Complete reaction of Phl + Qtz to En + Sa was observed in four experiments interpreted to be quite far from the equilibrium position. All other experiments except two (11 and PQ2 in Table 2) produced strong (>30%) changes in relative peak intensities, making interpretation of run direction unambiguous. The new experimental data bracket the equilibrium in pure H_2O between 755 and 769 °C at about 0.5 kbar, and in mixed volatiles at ~2.5, 2, and ~1.75 kbar, and are particularly constraining at the two latter pressures (runs 18 and 19; PQ1 and PQ3, respectively).

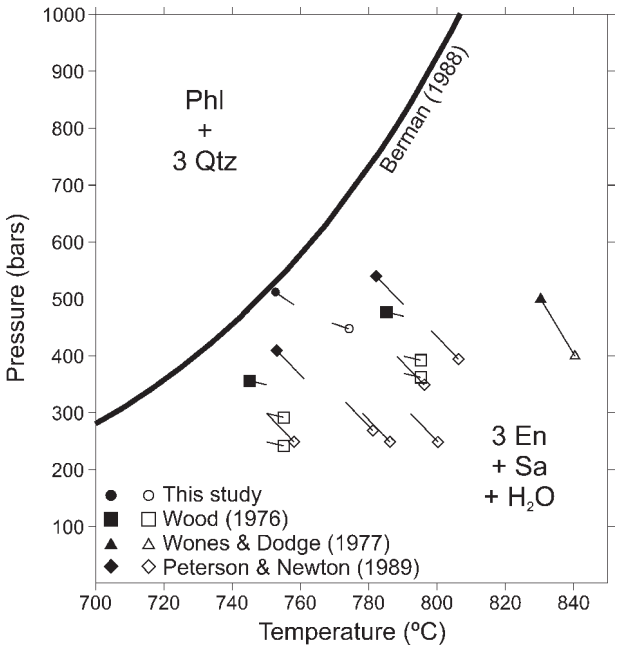

FIGURE 4. *P-T* diagram showing experimental data for Equilibrium 1 in pure H_2O along with its position calculated with thermodynamic data of Berman (1988; thick curve). Symbols show experimental data after adjustment for experimental uncertainties, and the ends of connected lines show nominal experimental conditions. Solid and open symbols show growth of low-*T* and high-*T* assemblages, respectively.

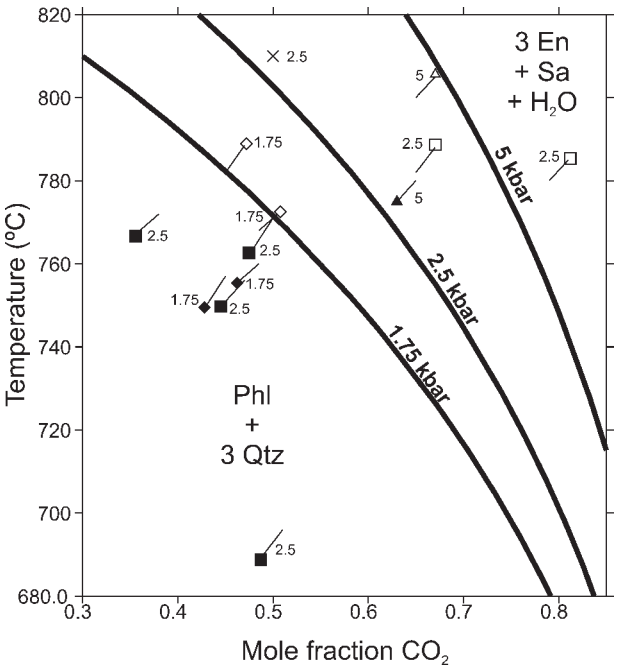

FIGURE 5. *T*-X_{CO_2} diagram showing experimental data for Equilibrium 1 along with its position at 1.75, 2.5, and 5 kbar, calculated with thermodynamic data of Berman (1988). Symbols as in Figure 4, with data from this study at 1.75 kbar (diamonds) and 2.5 kbar (squares), and from Bohlen et al. (1983) at 5 kbar (triangles). Numbers beside data points indicate pressure (kbar) of experiments.

Experimental data for Equilibria 2 and 3

Experimental half-brackets for Equilibria 2 and 3 are listed in Table 3. All run products contained fine-grained (2–15 μm) biotite along with Sil, Sa, Qtz, and H_2O with no additional phases (e.g., Fig. 6), except for experiments S5 and S6 in which biotite reacted to form cordierite + hercynite + melt. As in many other studies involving solid solutions (e.g., Perkins et al. 1981; Aranovich and Berman 1997; Benisek et al. 1996), the major difficulties in interpreting the results of these experiments stemmed from characterizing and interpreting the chemical heterogeneity of run products.

Analyses of 10–22 biotite grains were collected for each run sample, with oxide totals ranging between 49 and 96 wt%. Replicate analyses of the same biotite grains in synthesis and run products suggest that Al contents of individual grains are reproducible to ±0.04 Al pfu. Analyses utilized to define Al contents had K between 0.85–1.02 pfu (22 negative charge formula), and oxide totals between 68–91 and 83–96 wt% for Mg- and Fe-biotite, respectively. No correlation was discerned between calculated Al contents and analytical oxide sums. For example, of the 22 grains analyzed for experiment E26 (Table 3), 14 analyses with oxide totals greater than 85 wt% yielded total Al between 1.64–1.96, whereas 8 analyses with oxide totals less than 81 wt% gave total Al between 1.65–1.92. Thus, the low totals resulting from analysis of thin biotite flakes do not appear to have compromised results, whereas analysis of dispersed single grains ensured that results do not represent mixed analyses from more than one phase.

Although total Al contents could be determined with confidence, imprecision in Si analyses due to fine grain size and surface irregularities made it impossible to determine octahedral vs. tetrahedral Al contents unambiguously. The analytical data in both the Fe- and Mg-systems suggest some decoupling of octahedral and tetrahedral Al that can be expressed in terms of a Tschermak exchange [^{VI}Mg(Fe)^{IV}Si = ^{VI}Al^{IV}Al], relating Phl (Ann) and Eas (Sdr) components, and a dioctahedral-trioctohedral exchange [3^{VI}Mg(Fe) = 2^{VI}Al + ^{VI}□] relating Phl (Ann) and Ms components. Compositional trends in other experimental studies (Robert 1976; Patino Douce et al. 1993) and natural biotites (Guidotti 1984; Guidotti and Dyar 1991) can be interpreted similarly. Synthesis experiments suggest a maximum of about 8–10% Ms component in biotite at 600 °C (Rutherford 1973; Robert 1976), a value compatible with the present results.

All experimental runs produced biotite compositions that were significantly shifted from the starting compositions (Fig. 7). Core to rim zonation in biotite Al content was not discernible. The compositional variation between different grains in a single sample (Fig. 7) was generally in the range 0.2–0.4 Al pfu. These compositional shifts can be interpreted as differing degrees of approach toward equilibrium, with the most advanced Al content (the most different from that of the starting biotite) representing the closest appproach to the equilibrium value. A complicating factor, however, is the possible overstepping of equilibrium Al contents, as has been observed in experiments on Al solubility in orthopyroxene (e.g., Perkins et al. 1981). Two of the nine brackets that were obtained in our study show overlapping brackets that are larger than analytical uncertainties,

suggesting that the dominant mechanism of equilibration was dissolution and recrystallization, not diffusive reequilibration (e.g., Pattison 1994).

Tabulated Al values (Table 3) show the range of compositions analyzed in each run, with the most advanced side of this range representing the average of either 2 or 3 grains in each run product that were within analytical uncertainty (0.04 Al). Pairs of complementary experiments produced convergent compositional brackets (within 0.05 Al pfu), with the exception of two pairs of half-brackets that overlap by 0.05 (E23, E24 and S1, S2) Al pfu (Table 3, Fig. 7). Experimental data for the Phl–Eas join (Equilibrium 2) indicate that the assemblage Bt-Sil-Sa-Qtz-H_2O buffers the Al content of Mg-biotite to an approximately constant value, nominally 1.60 ± 0.04 Al pfu, over the *P-T* range 1.1–3.2 kbar and 647–755 °C (Table 3, runs E21–E30; Fig. 7a). Experimental data between 606–698 °C at ~2–3.5 kbar for the Ann–Sdr join (Equilibrium 3; Fig. 7c) demonstrate that the same assemblage buffers the Al content of Fe-biotite to a significantly greater value (nominally 2.08 ± 0.05 Al pfu) than in the Mg-system (Table 3, runs S1–S10, Fig. 7). The nominal data suggest a slight decrease in Al with increasing temperature (Fe–Al system; Fig. 7c) and decreasing pressure (Mg–Al and Fe–Al system). One experiment performed in the Fe–Mg system used starting materials with Fe/(Fe + Mg) = 0.50 and either 1.0 Al pfu (FM_{50}) or 2.6 Al pfu ($Sdr_{80/50}$). The compositions of run products converged within 0.05 Al pfu (Fig. 7b), but shifted to Fe/(Fe + Mg) = 0.43–0.44 ± 0.02 (Table 3) due to the crystallization of magnetite.

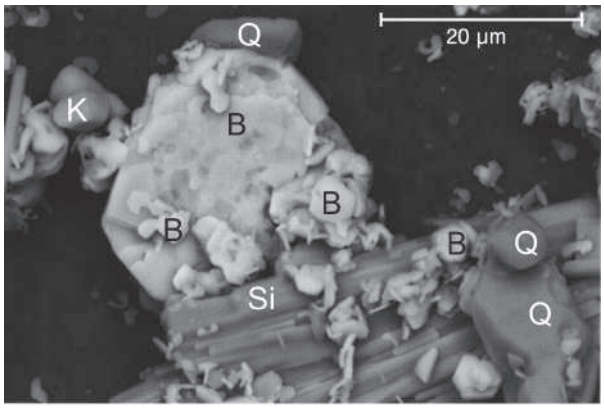

FIGURE 6. Secondary electron image of run product of experiment 8 for Equilibrium 3. Abbreviations: B = biotite; K = sanidine; Q = quartz; Si = sillimanite.

Experimental data for Equilibrium 4

Starting materials for these experiments used Sdr_{55}, the equilibrium biotite composition determined above (Equilibrium 3). Experimental data bracketing Equilibrium 4 were obtained at ~2.4 kbar (Table 4 and Fig. 8). All run products contained the assemblage Bt-Alm-Sil-Sa-Qtz-H_2O, with no additional phases identified by XRD, SEM, or optically. XRD patterns of run products showing strong biotite growth exhibit stronger peaks at 43.25° 2θ than the Sdr_{55} used in the starting materials. These peaks are close to the positions of (010) and (131) Ms peaks, but no muscovite was found in detailed SEM imaging, and all experiments were run at temperatures exceeding Ms + Qz stability. Consequently, we interpret this change to indicate an increase in the amount of Ms component in the product biotite.

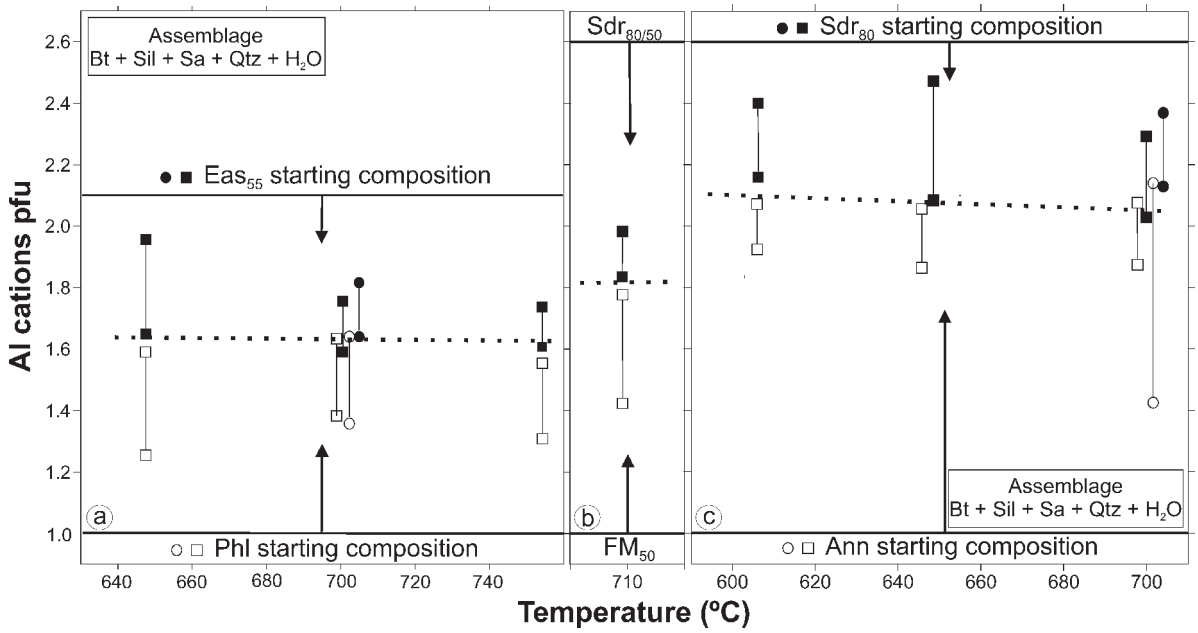

FIGURE 7. Al content buffered by Equilibria 2 and/or 3 of (**a**) Mg-Al, (**b**) Mg-Fe-Al, and (**c**) Fe-Al biotites determined in this study (Table 3). Paired symbols show the range of total Al observed in different biotite grains of the same run product. Open and closed symbols represent the results of experiments starting with low-Al biotite and high-Al biotite, respectively. Squares and circles represent lower and higher pressure data, respectively. Dotted curves show calculated Al contents at 2 kbar.

THERMODYNAMIC ANALYSIS

Methods

The experimental data presented in this paper provide fairly stringent constraints on the thermodynamic properties of biotite end-members (Phl, Ann, Eas, Sdr) since the properties of other phases (En, Alm, Qtz, Sa, Sil, H_2O, and H_2O-CO_2 mixtures) that participate in the studied equilibria are well known. The derived properties for Eas and Sdr are somewhat less certain because the amount of muscovite component (distribution of Al between octahedral and tetrahedral sites) could not be determined quantitatively in our experiments. However, as described below, the properties of Eas and Sdr are relatively insensitive to the exact partitioning of Al between tetrahedral and octahedral sites. Although lack of explicit incorporation of a muscovite component does compromise a complete thermodynamic description of Fe-Mg-Al biotite, the thermodynamic properties derived here for the above four end-members represent major improvements that are important for both forward and inverse petrologic modeling.

Thermodynamic analysis of experimental data for Equilibria 1–4 utilized the equations of state of Haar et al. (1984) for H_2O and Kerrick and Jacobs (1981) for H_2O-CO_2, along with thermodynamic properties of Berman (1988) for sanidine, quartz, and sillimanite. Thermodynamic properties of almandine and orthoenstatite, which participate in Equilibria 4 and 1, as well as olivine and garnet (see below), were taken from Berman and Aranovich (1996), who used the above thermodynamic data in their analysis of experimental data involving selected solid solutions (Grt, Opx, Ol, Crd, Ilm).

The technique of linear programming was used to derive thermodynamic data (Gordon 1973). With this technique, the thermodynamic equation for equilibrium can be expressed as an inequality:

$$\Delta G_{P,T} + \mathrm{R}T\ln K_X + \mathrm{R}T\ln K_\gamma < \text{or} > 0$$

where K_X and K_γ are the products of mole fraction terms (ideal activities, a^{id}) and activity coefficients, respectively, raised to the power of their reaction coefficients. $\Delta G_{P,T}$ is the standard state (unit activity of pure minerals at P and T) Gibbs free energy change of reaction at P and T, expressed by:

$$\Delta G_{P,T} = \Delta H_{1,298} - T\Delta S_{1,298} + \int_{298}^{T} \Delta C_P dT - T\int_{298}^{T} \frac{\Delta C_P}{T} dT + \int_{1}^{P} \Delta V \; dP .$$

Standard state properties (Table 5) for phlogopite, eastonite, annite, and siderophyllite, and biotite mixing properties (Table 6) were derived by analysis of experimental data for Equilibria 1–4 presented in this study, using an objective function that minimized the extent of nonideal mixing in biotite. In addition to constraints on heat capacities (Table 5), molar volumes (this study; Circone et al. 1991; Benisek et al. 1996), and entropies (see below), annite properties were anchored further by consideration of reversed Fe-Mg partitioning data between olivine and biotite (Zhou 1994). Using the same C-CH_4 buffer as employed in our study, Zhou defined K_D between 650–900 °C, with $Fe^{3+} = 10 \pm 2\%$ in biotite of starting materials and run products. Annite properties also were evaluated relative to phase-equilibrium constraints on annite stability using hydrogen sensors to monitor hydrogen fugacity (Cygan et al. 1996).

Experimental constraints on the site occupancy of Al in biotite differ between the Fe- and Mg-systems. Structural refinements for Fe-Al biotite demonstrate that Al occupies the two M2 sites (Redhammer et al. 2000; Redhammer and Roth 2002). In contrast, infrared and Raman spectra of Mg-Al-biotite indicate that ^{VI}Al orders onto the M1 site (Circone and Navrotsky 1992). In the present analysis of a fairly restricted experimental data set, we adopt the model in which ^{VI}Al orders onto the M1 site so that our results can be compared directly to the results of other experimental studies that were analyzed with this same model (e.g., Circone and Navrotsky 1992; Benisek et al. 1996).

Computer modeling of ^{29}Si NMR spectra for Mg-Al biotite led Circone et al. (1991) to formulate a model of short-range ordering of Al and Si over four tetrahedral sites (dominated by Al avoidance). As their data indicate an entropy of mixing much closer to that of Al-Si mixing on two T_1 sites than that of random mixing over four equivalent tetrahedral sites, we base our calculations on the two T_1 site model. This model implies a configurational entropy, $S_{config} = -2\mathrm{R}(X_{Si}\ln X_{Si} + X_{Al}\ln X_{Al})$, of 11.5 J/(mol·K) for phlogopite (annite), and zero for eastonite (siderophyllite). The random distribution of Al-Si over four tetrahedral sites yields $S_{config} = -4\mathrm{R}(X_{Si}\ln X_{Si} + X_{Al}\ln X_{Al}) = 18.7$ and 23.05 J/(mol·K) for phlogopite and eastonite, respectively. These configurational contributions to third law entropies are discussed in relation to the results of thermodynamic modeling below.

With the above assumptions, ideal activities of biotite end-members are:

$$a^{id}_{Phl} = 16X^{M1}_{Mg}(X^{M2}_{Mg})^2(X^{T1}_{Al})^2(X^{T1}_{Si})^2$$
$$a^{id}_{Ann} = 16X^{M1}_{Fe}(X^{M2}_{Fe})^2(X^{T1}_{Al})^2(X^{T1}_{Si})^2$$
$$a^{id}_{Eas} = X^{M1}_{Al}(X^{M2}_{Mg})^2(X^{T1}_{Al})^2$$
$$a^{id}_{Sdr} = X^{M1}_{Al}(X^{M2}_{Fe})^2(X^{T1}_{Al})^2$$

Nonideal mixing was accounted with on-site terms:

$$\mathrm{R}T\ln\gamma_{Phl} = \mathrm{R}T\ln\gamma^{M1}_{Mg} + 2\mathrm{R}T\ln\gamma^{M2}_{Mg}$$
$$\mathrm{R}T\ln\gamma_{Ann} = \mathrm{R}T\ln\gamma^{M1}_{Fe} + 2\mathrm{R}T\ln\gamma^{M2}_{Fe}$$
$$\mathrm{R}T\ln\gamma_{Eas} = \mathrm{R}T\ln\gamma^{M1}_{Al} + 2\mathrm{R}T\ln\gamma^{M2}_{Mg}$$
$$\mathrm{R}T\ln\gamma_{Sdr} = \mathrm{R}T\ln\gamma^{M1}_{Al} + 2\mathrm{R}T\ln\gamma^{M2}_{Fe}$$

using symmetric Margules parameters for Mg-Al and Fe-Al interactions on the M1 site and Fe-Mg interactions on the M1 and M2 sites (e.g., Berman 1990):

$$\mathrm{R}T\ln\gamma^{M1}_{Mg} = W^{M1}_{MgAl}(X^{M1}_{Al} - X^{M1}_{Al}X^{M1}_{Mg}) - W^{M1}_{FeAl}(X^{M1}_{Al}X^{M1}_{Fe}) + W^{M1}_{MgFe}(X^{M1}_{Fe} - X^{M1}_{Mg}X^{M1}_{Fe})$$
$$\mathrm{R}T\ln\gamma^{M1}_{Fe} = W^{M1}_{FeAl}(X^{M1}_{Al} - X^{M1}_{Al}X^{M1}_{Fe}) - W^{M1}_{MgAl}(X^{M1}_{Al}X^{M1}_{Mg}) + W^{M1}_{MgFe}(X^{M1}_{Mg} - X^{M1}_{Mg}X^{M1}_{Fe})$$
$$\mathrm{R}T\ln\gamma^{M1}_{Al} = W^{M1}_{MgAl}(X^{M1}_{Mg} - X^{M1}_{Al}X^{M1}_{Mg}) + W^{M1}_{FeAl}(X^{M1}_{Fe} - X^{M1}_{Al}X^{M1}_{Fe}) - W^{M1}_{MgFe}(X^{M1}_{Mg}X^{M1}_{Fe})$$
$$2\mathrm{R}T\ln\gamma^{M2}_{Mg} = W^{M2}_{MgFe}(X^{M2}_{Fe} - X^{M2}_{Mg}X^{M2}_{Fe})$$
$$2\mathrm{R}T\ln\gamma^{M2}_{Fe} = W^{M2}_{MgFe}(X^{M2}_{Mg} - X^{M2}_{Mg}X^{M2}_{Fe}).$$

Ferric iron in biotite and almandine was incorporated explicitly based on the values discussed above (see Table 1). Structural

TABLE 5. Standard state (1 bar, 298.15 K) thermodynamic properties of biotite end-members

	ΔH J/mol	S J/(mol·K)	V J/bar	k_0	k_1	$k_2 \times 10^{-6}$	$k_3 \times 10^{-8}$	C_P*
Phlogopite	–6215.86	327.26	14.97	610.38	–2083.78	–21.533	28.410	1
Annite	–5146.10	416.50	15.46	666.90	–3354.51	–17.319	25.197	2
Eastonite	–6324.95	318.59	14.74	619.79	–2272.34	–22.291	30.047	2
Siderophyllite	–5621.14	378.09	15.06	657.49	–3119.92	–19.481	27.904	2

Notes: For all end-members (Berman 1988): $V_{P,T}/V_{1,298} = 1 - 1.697 \times 10^{-6} (P - 1) + 34.447 \times 10^{-5} (T - 298.15)$. For Equilibrium 5, $\Delta H = -9.4$ kJ/mol; $\Delta S = \Delta V = 0$.
*$C_P = k_0 + k_1 T^{-0.5} + k_2 T^{-2} + k_3 T^{-3}$ [J/(mol·K)]. 1 = Berman (1988). 2 = Estimated with C_P model of Berman and Brown (1985) for equations: Ann = Phl – 3MgO + 3FeO; Eas = Phl – MgO – SiO_2 + Al_2O_3; Sid = Eas + 2/3 Ann – 2/3 Phl.

TABLE 6. Biotite mixing properties

Parameter	W_H (kJ/mol)
W^{M1}_{MgFe}	1.0
W^{M2}_{MgFe}	2.0
W^{M1}_{FeAl}	–8.2
W^{M1}_{MgAl}	0

formulae for experimentally equilibrated biotite were calculated assuming that total Al contents stem from a Tschermak (siderophyllite, eastonite) substitution without a muscovite component (see above). Importantly, derived thermodynamic properties are insensitive to this assumption because of the compensating effect on calculated ideal activities of transferring Al between octahedral and tetrahedral sites. For example, the ~2.08 total Al pfu determined for Fe-biotite at 2 kbar and 647 °C (Table 3) can be represented as $X_{Sdr} = 0.54$, which leads to $X^{M1}_{Al} = 0.54$ and $X^{T1}_{Al} = 1.54/2 = 0.77$, and a contribution to $RT\ln a^{id}_{Sdr}$ of $RT\ln[(0.54)(0.77)^2] = -8523$ J/mol at 900 K. Representing the 2.08 total Al pfu with 10% Ms and 90% Sdr components, leads to $X^{M1}_{Al} = 0.64$, $X^{M2}_{\square} = 0.1/2 = 0.05$, $X^{T1}_{Al} = 1.44/2 = 0.72$, and a contribution to $RT\ln a^{id}_{Sdr}$ of $RT\ln[(0.64)(0.72)^2] = -8256$ J/mol at 900 K, an energy difference of only 267 J/mol.

Phlogopite stability

Our high-T half-bracket for Equilibrium 1 in pure H_2O (experiment no. 20 in Table 2; Fig. 4) contradicts the results of Wood (1976) and Wones and Dodge (1977), whereas our data with a H_2O-CO_2 fluid (Fig. 5) are consistent with the 5 kbar bracket of Bohlen et al. (1983). Particularly constraining is our half-bracket at 1.74 kb and 768 °C (experiment no. 18, Table 2), which when analyzed with experiment no. 22 in pure H_2O, limits $S^{Phl}_{1,298}$ to be less than 327.7 J/(mol·K). The bracket of Bohlen et al. (1983) further limits $S^{Phl}_{1,298}$ to 327.5 J/(mol·K), whereas data of Aranovich and Newton (1998) using H_2O-KCl fluids are narrowly more constraining, leading to $S^{Phl}_{1,298} = 327.3$ J/(mol·K). Compared to the calorimetrically derived third law entropy, 315.9 J/(mol·K), the retrieved value is congruent with Al-Si disorder over two tetrahedral sites [11.5 J/(mol·K) contribution]. These results are dependent, however, on Berman's (1988) entropy of sanidine, which incorporates less than the maximum configurational entropy of disorder on tetrahedral sites [15.0 vs. 18.7 J/(mol·K)]. The combined data for Equilibrium 1 define the standard enthalpy of formation of phlogopite at –6215.86 kJ/mol, in excellent agreement with the solution-calorimetric value (–6215 ± 3.5 kJ/mol) measured by Circone and Navrotsky (1992).

Our new experimental data on Equilibrium 1 indicate a significantly reduced thermal stability of phlogopite + quartz over the older data of Wood (1976) and Wones and Dodge (1977), as concluded in the analysis of Berman (1988). Graphchikov et al. (1999) have argued that the Wood's (1976) position of the Equilibrium 1 in pure H_2O is supported by the experiments of Clemens (1995). Indeed, a single datum on Equilibrium 1 reported by Clemens (between 0.51 and 0.62 kbar at 800 ± 5 °C) appears to support the early results of Wood (1976). However, the datum of Clemens is not a true reversal, as only traces of phlogopite and no quartz were observed in the phlogopite + quartz producing half-bracket (Clemens 1995, Table 2, run K-37).

Thermodynamic properties of Mg-Al biotite

The experimental data for Equilibrium 2 constrain Al solubility in Mg-biotite, and provide constraints on the thermodynamic properties of eastonite. Assuming ideal Mg-Al mixing, and with phlogopite properties constrained as discussed above, the phase-equilibrium data allow $S^{Eas}_{1,298}$ to vary between 306 J/(mol·K) (the value estimated by the method of Holland 1989) and 329.05 J/(mol·K), the value associated with full disorder of Al and Si on 4 tetrahedral sites. The minimum standard enthalpy of formation of eastonite (–6337.4 kJ/mol) is approximately 15 kJ/mol more positive than the maximum value (–6352 to –6363 kJ/mol) obtained by solution calorimetry (Circone and Navrotsky 1992). Circone and Navrotsky (1992) measured a strong positive deviation from ideality (22.8 kJ/mol for a symmetric regular solution parameter, W_{MgAl}) from their drop-calorimetry results on Mg-Al-biotite with up to 0.92 octahedral Al. With the constraints imposed by the standard-state entropy and volume of Equilibrium 2, the reversed compositional brackets for Equilibrium 2 impose an upper limit of 12.8 kJ/mol for W^{M1}_{MgAl} on this join. It is interesting to note that, within uncertainties, the heat of solution measurements are linear with composition up to $Phl_{20}Eas_{80}$, with only the most aluminous ($Phl_{08}Eas_{92}$) sample deviating strongly from this trend. If this sample, which also deviates most strongly from the accepted linear relationship between volume and composition (Circone et al. 1991), is omitted, the Circone and Navrotsky (1992) data are compatible with ideal mixing on this join as well as with the standard enthalpy of formation of eastonite based on phase equilibrium data for Equilibrium 2.

Thermodynamic properties of Fe-Al biotite

Experimental data defining Al solubility in Fe-biotite via Equilibrium 3 provide constraints on the thermodynamic properties of siderophyllite relative to annite. With these constraints, experimental data defining Fe-biotite + sillimanite + quartz stability relative to almandine + sanidine + H_2O via Equilibrium 4 allow annite properties and the extent of nonideality on the Ann–Sdr join to be evaluated, but not independently. For example, the data for these two equilibria limit W^{M1}_{FeAl} to the range –15.2 to

–2.3 kJ/mol. If annite properties are constrained independently by Fe-Mg partitioning data between olivine and biotite (Zhou 1994), which are well reproduced with $W^{Ol}_{MgFe} = 10.4 - 0.004T$ kJ/mol (Berman and Aranovich 1996) and $W^{M1,Bt}_{MgFe} = W^{M2,Bt}_{MgFe}/2 = 1.0$ kJ/mol, W^{M1}_{FeAl} is constrained between –11.5 to –6.1 kJ/mol. This result is significantly greater than the –29.4 kJ/mol value derived by Benisek et al. (1996) on the basis of experimental displacement of the equilibrium:

$$Ann = Sa + Mt + H_2. \quad (6)$$

The more negative value obtained by Benisek et al. (1996) is related to their acceptance of Dachs' (1994) position of the end-member Equilibrium 6, which yields a much smaller stability field for annite than determined in other experimental studies (Eugster and Wones 1962; Hewitt and Wones 1984; Cygan et al. 1996) and in our thermodynamic analysis. One reason for an experimental discrepancy may be the very short run duration of Dachs' experiments (see Table 1 of Dachs 1994), insufficient to equilibrate the sluggishly reacting Ann+Sa+Mt+H_2O assemblage. That this was the case is suggested by the highly time-dependent values of the final f_{H_2} obtained by Dachs in the three runs of variable duration at 750°C (see also the discussion of Dachs' experiments by Cygan et al. 1996 and Chou 1997).

Additional support for the annite properties derived here comes from comparison with the reversed phase-equilibrium data of Cygan et al. (1996) for the equilibrium:

$$annite = sanidine + magnetite + H_2.$$

The data derived here successfully reproduce their equilibrium curve at temperatures above 750 °C, which are associated with the most reducing conditions and the least Fe^{3+} in annite (6 to 15 ± 5% of total Fe; Cygan et al. 1996). These calculations are relatively insensitive to various assumptions regarding the energetics of, or the precise amount of this small amount of oxyannite component, the substitution mechanisms of which have been studied in detail by Rancourt et al. (2001).

With annite properties constrained by the Ol-Bt exhange data (Zhou 1994), as discussed above, the combination of experimental data for Equilibria 3 and 4 place constraints on the third law entropy of siderophyllite, $S^{Sdr}_{1,298}$. The maximum value is 387 J/(mol·K), which, in comparison to the estimated third law entropy of siderophyllite [365 ± 3 J/(mol·K); Holland 1989], corresponds to full disorder over four tetrahedral sites. The minimum value is 371.6 J/(mol·K), with values greater than 377 J/(mol·K) most compatible with the nominal experimental data. Thus, the experimental data are inconsistent with Al-Si mixing on two T_1 sites ($S_{config} = 0$ for siderophyllite), but are consistent with the short-range ordering of Al-Si over four tetrahedral sites (Circone et al. 1991; Circone and Navrotsky 1992).

Discussion

Comparison with natural data

Although detailed investigation has revealed differences in octahedral cation ordering between synthetic and natural Fe-bearing biotite (Mercier et al. 2005), we expect that the magnitude of these differences does not significantly affect application of our experimental data to naturally occurring biotite. To compare the Al contents determined in this study with natural data, assumptions must be made regarding minor element octahedral and tetrahedral site substitutions in natural biotites, particularly Ti and Fe^{3+}. Fe-rich biotites coexisting with sillimanite generally contain about 1.75 Al pfu (Cheney and Guidotti 1975; Guidotti 1984), with $Fe^{3+} \sim 0.15$ (assuming $Fe^{3+} = 12\%$ of total Fe, Guidotti and Dyar 1991), and Ti ~ 0.1–0.2. The sum of these components (~2.05) is almost identical to the Al values (~2.08) determined in the Fe-system (Table 3). Crystal-chemical arguments (Bailey 1984) indicate that Ti and some Fe^{3+} are octahedrally coordinated in biotite, and the above comparison suggests that these components may compete directly with Al for occupancy on the octahedral sites. Natural Mg-rich biotites coexisting with Sil or staurolite contain 1.65–1.70 Al (Cheney and Guidotti 1975), slightly greater than the value (1.60 Al) determined experimentally in the Mg-system (Table 3). The small difference can again be attributed to the amount of octahedral Ti and Fe^{3+} in natural Mg-rich biotites (each about 0.05 cations/12 anions, Cheney and Guidotti 1975). Biotite with intermediate Fe/(Fe + Mg) ratios from Al-saturated pelitic assemblages (Guidotti and Dyar 1991; Holdaway et al. 1997) range between 1.6–1.8 Al pfu, in accord with our experimental results if Fe^{3+} and Ti are accounted for in the natural biotite.

Analyses of natural biotite coexisting with sillimanite show that total Al does not vary with temperature, but the amount of muscovite component increases with increasing temperature (Guidotti and Dyar 1991). This correlation requires that siderophyllite and eastonite components are negatively correlated with temperature. Due to compositional uncertainties and the small temperature range of our experiments, we were not able to discern a temperature dependence for Al solubility. However, the nominal data suggest, and our derived thermodynamic properties predict, the inverse temperature correlation inferred from the natural analyses. The calculated temperature dependence is small, however, with total Al pfu decreasing by 0.04 and 0.01 in the Fe- and Mg-systems, respectively, over a temperature interval of approximately 100 °C.

Predicted phase relations

The thermodynamic properties of siderophyllite, derived from experimental data on Equilibrium 3, can be used to compute the equilibrium Al content of Fe-biotite as a function of P and T, evaluate the effect of Al solubility on Fe-biotite stability, and compare to available experimental data. Figure 8 shows the results for the upper temperature stability of the assemblage Fe-biotite + sillimanite + quartz, calculated with the program THERIAK (de Capitani and Brown 1987; http://titan.minpet.unibas.ch/minpet/theriak/theruser.html). At low P, the breakdown curve corresponds to the univariant reaction:

$$2\,Ann_x Sdr_{(1-x)} + (6-4x)\,Sil + (9+x)\,Qz = (3-x)\,fCd + 2\,Sa + 2\,H_2O. \quad (7)$$

At pressures exceeding hydrous fCd stability (about 2.4 kbar), the breakdown reaction corresponds to:

$$3\,Ann_x Sdr_{(1-x)} + (3-4x)\,Sil + (6+4x)\,Qz = (3-x)\,Alm + 3\,Sa + 3\,H_2O. \quad (4')$$

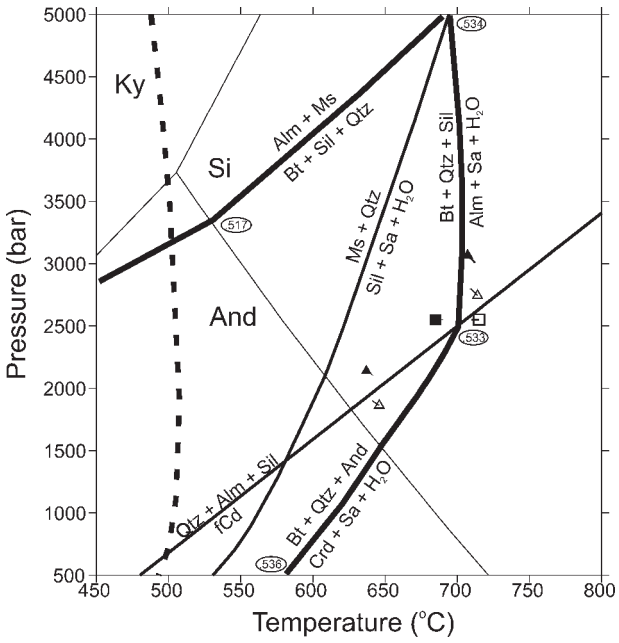

FIGURE 8. *P-T* diagram showing equilibria and mineral compositions computed with thermodynamic data derived from reported experimental data (Table 5). Numbers beside calculated curves are number of octahedral Al pfu. Symbols show experimental brackets for Bt + Sil + Qtz breakdown to Alm + Sa + H_2O (squares; this study) and to Crd + Sa + H_2O (triangles; Holdaway and Lee 1977). Dashed curve shows position of the equilibrium: Ann + Sil + Qtz = Alm + Sa + H_2O.

Octahedral Al in biotite (expressed as x, mole fraction of the Sdr end-member, in the above equilibria) changes slowly as P and T increase along the breakdown curves (Fig. 8). Compared to the computed position for Equilibrium 4 with pure annite ($x = 0$, dashed curve in Fig. 8), excess Al solubility in biotite stabilizes the biotite assemblage by approximately 200 °C!

Our computed curve for Equilibrium 7 is in accord with Holdaway and Lee's (1977) bracket at 710 °C (Fig. 8), but outside their 650 °C bracket. The agreement at high temperature suggests that their biotite, which was synthesized with a non-equilibrium Al content, likely crystallized with the equilibrium composition during their high-T experimental runs. The hercynite impurities present in their starting materials may have significantly affected their interpretation of run direction at 650 °C.

A somewhat surprising result of calculations in the Mg-system is that the mineral assemblage Bt-Sil-Sa-Qtz used to study Equilibrium 2 is metastable with respect to the Crd-Sa assemblage over the P-T range of our experiments. The lack of cordierite detected by XRD or SEM analysis of the experimental products suggests that kinetic factors inhibited cordierite growth.

The thermodynamic properties derived for biotite end-members and mixing permit the equilibrium Al content, and hence stability of Mg-Fe-Al biotite to be predicted as a function of P, T, and bulk composition (using cross-site corrections discussed below). These calculations are particularly important to incorporate into forward petrologic modeling that is increasingly being utilized to elucidate the quantitative P-T-t evolution of metamorphic rocks (e.g., Wei and Powell 2003; Berman et al. 2005). A major challenge for future work is the acquisition of reversed experimental data involving Mg-Fe-Al biotite that can be used to assess the accuracy of such predictions and to constrain further modeling.

Implications for geothermobarometry

The combined set of experimental data (Equilibria 1–4) constraining the thermodynamic properties of the four biotite end-members provide a tight bracket on the Gibbs free energy of the internal equilibrium:

$$2/3\ \mathrm{Ann} + \mathrm{Eas} = 2/3\ \mathrm{Phl} + \mathrm{Sdr}. \quad (5)$$

For example, $\Delta H_{1,298}(5)$ is bracketed between –9.3 and –11.0 (optimal value = –9.4 kJ/mol; Table 5), assuming $\Delta S = \Delta V = 0$, and ideal Mg-Al mixing. The stability of the Phl + Sdr assemblage reflects the strong affinity of Al for Fe in biotite, as previously deduced for biotite and other minerals (e.g., Aranovich 1991; Mader et al. 1994; Berman and Aranovich 1996). This Fe-Al affinity has major implications for geothermobarometry, as illustrated below with the example of the garnet-biotite Fe-Mg exchange thermometer:

$$\mathrm{Ann} + \mathrm{Py} = \mathrm{Alm} + \mathrm{Phl}. \quad (8)$$

The energetics of Mg, Fe, and Al mixing has typically been modeled with nonideal on-site interactions (e.g., Indares and Martingole 1985; Patino Douce et al. 1993). An alternative approach is calculation of activity coefficient corrections on the basis of cross-site terms applied to the energetics of internal equilibria among end-members of a solid solution (e.g., Wood and Nicholls 1978; Aranovich et al. 1988; Aranovich 1991). Although recent analyses of structural refinement data for single crystals of biotite indicate size differences between M1 and M2 that likely reflect cation ordering (Mercier et al. 2005), available data for Fe-Mg biotite demonstrate very limited octahedral site partitioning (Redhammer and Roth 2002). Assuming equal Fe-Mg partitioning on the Ann-Phl binary (no octahedral Al), the cross-site corrections are given by:

$$R T \ln\gamma_{r,\mathrm{Phl}} = -\Delta G_5 X^{M2}_{Fe} X^{M1}_{Al}$$
$$R T \ln\gamma_{r,\mathrm{Ann}} = \Delta G_5 X^{M2}_{Mg} X^{M1}_{Al}$$
$$R T \ln\gamma_{r,\mathrm{Eas}} = \Delta G_5 X^{M2}_{Fe}(1 - X^{M1}_{Al})$$
$$R T \ln\gamma_{r,\mathrm{Sdr}} = -\Delta G_5 X^{M2}_{Mg}(1 - X^{M1}_{Al})$$

The garnet-biotite exchange thermometer 8 can be calibrated by combining the thermodynamic properties of biotite extracted here (Table 5) with those of garnet derived by Berman and Aranovich (1996). This calibration successfully reproduces the Fe-Mg exchange data of Ferry and Spear (1978) if approximately 6% Fe^{3+} is assumed in the experimental biotite. The potential magnitude of the activity coefficient correction can be appreciated with reference to aluminous biotite that occurs with garnet, andalusite, and sillimanite in metapelitic rocks studied by Ferry (1980). For sample 666, with $X_{Al} = 0.52$ (assuming one octahedral site), the calculated temperature with Equilibrium 8 is 65 °C lower using the activity coefficient correction. These results

discriminate between proposed Margules models, corroborating those that produce similar temperature effects with $W_{FeAl} < W_{MgAl}$ (e.g., Indares and Martingole 1985, and many others since), and contradicting those with $W_{MgAl} < W_{FeAl}$ (e.g., Hoisch 1990; Patino Douce et al. 1993).

An additional implication of the experimental data presented here is that they provide improved calibration of barometers involving siderophyllite or eastonite. For example, Hoisch (1990) first suggested use of the equilibrium:

$$3\ \mathrm{Ann} + 6\ \mathrm{An} = 3\ \mathrm{Sdr} + 6\ \mathrm{Qz} + \mathrm{Grs} + \mathrm{Alm} \quad (9)$$

to compute equilibration pressures of aluminosilicate- and muscovite-absent metasedimentary rocks containing the relatively common assemblage garnet-biotite-plagioclase-quartz. The calibrations of Equilibrium 9 provided by Hoisch (1990), and recently Wu et al. (2004), are strictly empirical, based on regression analysis of natural mineral compositions against *P-T* values estimated with other available thermobarometers. The siderophyllite properties derived in this study permit direct calibration of the standard-state properties of Equilibrium 9, and thus provide more reliable application of this barometer. As with any biotite-bearing equilibria, successful applications over a range of metamorphic grade require calibration of the effects of, not only Al (discussed above), but also Ti, which varies from close to zero at greenschist facies to $X_{Ti} = 0.5$ at granulite facies (e.g., Guidotti and Dyar 1991). Description of the calibration of the energetics of Ti mixing in biotite is, however, beyond the scope of this paper. Such documentation, as well as the thermodynamic properties of biotite calibrated via consideration of constraints from natural assemblages in addition to a more extensive experimental data set than considered in this paper can be accessed with version 2.30 of the TWQ software (http://gsc.nrcan.gc.ca/sw/twq_e.php).

ACKNOWLEDGMENTS

The results presented in this contribution could not have been obtained without the generous technical support of many GSC personnel to whom we extend our most sincere gratitude: Steve Banszky and Sean Going who ensured that the lab stayed fully operational, John Stirling for assistance with microprobe analysis, Armand Tsai for his patient SEM work, and Bob Dilabio for running many XRD scans. We also thank Corinne Bensimon of the University of Ottawa who collected some of the XRD data for cell refinements. Helpful reviews were supplied by B. Kjarsgaard, T. Gordon, A. Patino Douce, and E. Ghent. Financial support was received from RFBR grant no. 03-05-64641 (to L.Y.A.), NSF grant no. EAR-9632591 (to R.C. Newton, U of Chicago), and NSERC Discovery Grant (to D.G.R.). This is ESS contribution no. 20060161.

REFERENCES CITED

Appleman, D.E. and Evans, T.H., Jr. (1973) Indexing and least-squares refinement of powder diffraction data, 26 p. U.S. Geological Survey Computer Contribution 20, National Technical Information Services, U.S. Department Commerce, Springfield, Virginia.

Aranovich, L.Y. (1991) Mineral equilibria of multicomponent solid solutions. Nauka Press, Moscow.

Aranovich, L.Y. and Berman, R.G. (1997) A new garnet-orthopyroxene thermometer based on reversed Al_2O_3 solubility in FeO-Al_2O_3-SiO_2 orthopyroxene. American Mineralogist, 97, 331–342.

Aranovich, L.Y. and Newton R.C. (1998) Reversed determination of the reaction: phlogopite + quartz = enstatite + potassium feldspar + H_2O in the range 750–875 °C and 2–12 kbar at low H_2O activity with concentrated KCl solutions. American Mineralogist, 83, 193–204.

Aranovich, L.Y., Lavrent'eva, I.V., and Kosyakova, N.A. (1988) Calibration of the biotite-garnet and biotite-orthopyroxene geothermometers corrected for the variable Al level in biotite. Geochemistry International, 25, 50–59.

Bailey, S.W. (1984) Crystal chemistry of the true micas. In S.W. Bailey, Ed., Micas, 13, p. 13–60. Reviews in Mineralogy, Mineralogical Society of America, Chantilly, Virginia.

Benisek, A., Dachs, E., Tippelt, G., Redhammer, G., and Amthauer, G. (1996) Activity-composition relationship in Tschermak's substituted Fe biotites at 700 °C, 2 kbar. Contributions to Mineralogy and Petrology, 125, 85–99.

Berman, R.G. (1988) Internally-consistent thermodynamic data for minerals in the system Na_2O-K_2O-CaO-MgO-FeO-Fe_2O_3-Al_2O_3-SiO_2-TiO_2-H_2O-CO_2. Journal of Petrology, 29, 445–522.

——— (1990) Mixing properties of Ca-Mg-Fe-Mn garnets. American Mineralogist, 75, 328–344.

Berman, R.G. and Aranovich, L.Y. (1996) Optimized standard state and mixing properties of minerals: I. Model calibration for olivine, orthopyroxene, cordierite, garnet, and ilmenite in the system FeO-MgO-CaO-Al_2O_3-SiO_2-TiO_2. Contributions to Mineralogy and Petrology, 126, 1–25.

Berman, R.G. and Brown, T.H. (1985) The heat capacity of minerals in the system Na_2O-K_2O-CaO-MgO-FeO-Fe_2O_3-Al_2O_3- SiO_2-TiO_2-H_2O-CO_2: representation, estimation, and high-temperature extrapolation. Contributions to Mineralogy and Petrology, 85, 168–183.

Berman, R.G., Aranovich, L.Y., and Rancourt, D. (1995a) Phase equilibrium constraints on the stability of biotite: Fe-Al biotite in the system K_2O-FeO-Al_2O_3-SiO_2-H_2O. Current Research of the Geological Survey of Canada 1995-E, 263–270.

Berman, R.G., Aranovich, L.Y., Genkin, M., and Mader, U.K. (1995b) Phase equilibrium constraints on the stability of biotite: Mg-Al biotite in the system K_2O-MgO-Al_2O_3-SiO_2-H_2O-CO_2. Current Research of the Geological Survey of Canada 1995-E, 253–261.

Berman, R.G., Sanborn-Barrie, M., Stern, R., and Carson, C. (2005) Tectonometamorphism at ca. 2.35 and 1.85 Ga in the Rae domain, western Churchill Province, Nunavut, Canada: insights from structural, metamorphic, and in situ geochronological analysis of the southwestern Committee Bay belt. Canadian Mineralogist, 43, 409–442.

Bohlen, S.R., Wall, V.J., and Clemens, J.D. (1983) Stability of phlogopite-quartz and sanidine-quartz: a model for melting in the lower crust. Contributions to Mineralogy and Petrology, 83, 270–277.

Cheney, J.T. and Guidotti, C.V. (1975) Interrelationship between Mg/Fe ratio and octahedral Al content in biotite. American Mineralogist, 60, 849–853.

Chou, I.M. (1987) Calibration of the graphite-methane buffer using the f_{H_2} sensors at 2 kbar pressure. American Mineralogist, 72, 76–81.

——— (1997) The use and misuse of H_2 sensors; a discussion of the paper by Dachs (1994). Contributions to Mineralogy and Petrology, 128, 302–305.

Chou, I.M. and Cygan, G.L. (1990) Quantitative redox control and measurement in hydrothermal experiments. In R.J. Spenser and I.M. Chou, Eds., Fluid-mineral interactions: a tribute to H.P. Eugster. Special Publication—Geochemical Society, 2, 3–15.

Circone, S. and Navrotsky, A. (1992) Substitution of $^{[6,4]}$Al in Phlogopite: High-temperature solution calorimetry, heat capacities, and thermodynamic properties of the phlogopite–eastonite join. American Mineralogist, 77, 1191–1205.

Circone, S., Navrotsky, A., Kirkpatrick, R.J., and Graham, C.M. (1991) Substitution of $^{[6,4]}$Al in Phlogopite: mica characterization, unit-cell variation, ^{27}Al and ^{29}Si MAS-NMR spectroscopy, and Al-Si distribution in the tetrahedral sheet. American Mineralogist, 76, 1485–1501.

Clemens, J.D. (1995) Phlogopite stability in the silica-saturated portion of the system $KAlO_2$-MgO-SiO_2-H_2O: New data and reappraisal of phase relations to 1.5 GPa. American Mineralogist, 80, 982–997.

Cygan, G.L., Chou, I.M., and Sherman, D.M. (1996) Reinvestigation of the annite = sanidine+magnetite+H_2 reaction using the f_{H_2}-sensor technique. American Mineralogist, 81, 475–484.

Dachs, E. (1994) Annite stability revised; 1, Hydrogen-sensor data for the reaction annite = sanidine + magnetite + H_2. Contributions to Mineralogy and Petrology, 117, 229–240.

Dachs, E. and Benisek, A. (1995) The stability of annite + quartz; reversed experimental data for the reaction 2 annite + 3 quartz = 2 sanidine + 3 fayalite + 2 H_2O. Contributions to Mineralogy and Petrology, 121, 380–387.

de Capitani, C. and Brown, T.H. (1987) The computation of chemical equilibrium in complex systems containing non-ideal solutions. Geochimica et Cosmochimica Acta, 51, 2639–2652.

Eugster, H.P. and Skippen, G.B. (1967) Igneous and metamorphic reactions involving gas equilibria. In P.H. Abelson, Ed., Researches in Geochemistry, p. 377–396. Wiley, New York.

Eugster, H.P. and Wones, D.R. (1962) Stability relations of the ferruginous biotite, annite. Journal of Petrology, 3, 82–125.

Ferry, J.M. (1980) A comparative study of geothermometers and geobarometers in pelitic schists from South-central Maine. American Mineralogist, 65, 720–732.

Ferry, J.M. and Spear, F.S. (1978) Experimental calibration of the partitioning of Fe and Mg between biotite and garnet. Contributions to Mineralogy and Petrology, 66, 113–117.

Goldsmith, J.R. and Jenkins, D.M. (1985) The hydrothermal melting of low and high albite. American Mineralogist, 70, 924–933.

Gordon, T.M. (1973) Determination of internally consistent thermodynamic data

from phase equilibrium experiments. Journal of Geology, 81, 199–208.
Graphchikov, A.A., Konilov, A.N., and Clemens, J.D. (1999) Biotite dehydration, partial melting, and fluid composition: Experiments in the system $KAlO_2$-FeO-MgO-SiO_2-H_2O-CO_2. American Mineralogist, 84, 15–26.
Guidotti, C.V. (1984) Micas in metamorphic rocks. In S.W. Bailey, Ed., Micas, 13, p. 357–468. Reviews in Mineralogy, Mineralogical Society of America, Chantilly, Virginia.
Guidotti, C.V. and Dyar, M.D. (1991) Ferric iron in metamorphic biotite and its petrologic and crystallochemical implications. American Mineralogist, 76, 161–175.
Haar, C., Gallagher, J.S., and Kell, G.S. (1984) NBS/NRC Steam Tables. Thermodynamic and transport properties and computer programs for vapor and liquid states of water in SI units. Hemisphere Publishing Co., Washington.
Hewitt, D.A. and Wones, D.R. (1975) Physical properties of some synthetic Fe-Mg-Al trioctahedral biotites. American Mineralogist, 60, 854–862.
——— (1984) Experimental phase relations of the micas. In S.W. Bailey, Ed., Micas, 13, p. 201–256. Reviews in Mineralogy, Mineralogical Society of America, Chantilly, Virginia.
Hoisch, T.D. (1990) Empirical calibration of six geobarometers for the mineral assemblage quartz+muscovite+biotite+plagioclase+garnet. Contributions to Mineralogy and Petrology, 104, 225–234.
Holdaway, M.J. and Lee, S.M. (1977) Fe-Mg cordierite stability in high-grade pelitic rocks based on Experimental, theoretical, and natural observations. Contributions to Mineralogy and Petrology, 63, 175–198.
Holdaway, M.J., Mukhopadhyay, B., Dyar, M.D., Guidotti, C.V., and Dutrow, B.L. (1997) Garnet-biotite geothermometry revised; new Margules parameters and a natural specimen data set from Maine. American Mineralogist, 82, 582–595.
Holland, T.J.B. (1989) Dependence of entropy on volume for silicate and oxide minerals: a review and a predictive model. American Mineralogist, 74, 5–13.
Hovis, G.L. (1989) Effect of Al-Si distribution on the powder-diffraction maxima of alkali feldspars and an easy method to determine T1 and T2 site occupancies. Canadian Mineralogist, 27, 107–118.
Indares, A. and Martingole, J. (1985) Biotite-garnet geothermometry in the granulite facies: the influence of Ti and Al in biotite. American Mineralogist, 70, 272–278.
Johannes, W. (1969) An experimental investigation of the system MgO-SiO_2-H_2O-CO_2. American Journal of Science, 267, 1083–1104.
Kerrick, D.M. and Jacobs, G.K. (1981) A modified Redlich-Kwong equation for H_2O, CO_2, and H_2O-CO_2 mixtures at elevated pressures and temperatures. American Journal of Science, 281, 735–767.
Kretz, R. (1983) Symbols for rock-forming minerals. American Mineralogist, 68, 277–279.
Mader, U.K., Percival, J.A., and Berman, R.G. (1994) Thermobarometry of garnet-clinopyroxene-hornblende granulites from the Kapuskasing structural zone. Canadian Journal of Earth Sciences, 31, 1134–1145.
Mercier, P.H.J., Rancourt, D.G., Robert, J.L., Berman, R.G., and Redhammer, G.J. (2005) Fundamental difference between synthetic powder and natural or synthetic single-crystal 1*M* micas; geometric homo-octahedral vs. geometric meso-octahedral sheets. American Mineralogist, 90, 399–410.
Partin, E. (1984) Ferric/ferrous determinations in synthetic biotite. M.S. thesis, Virginia Polytechnic Institute, Blacksburg.
Patino Douce, A.E., Johnston, A.D., and Rice, J.M. (1993) Octahedral excess mixing properties in biotite: a working model with applications to geobarometry and geothermometry. American Mineralogist, 78, 113–131.
Pattison, D.R.M. (1994) Are reversed Fe-Mg exchange and solid solution experiments really reversed? American Mineralogist, 79, 938–950.
Pattison, D.R.M. and Tracy, R.J. (1991) Phase equilibria and thermobarometry of metapelites. In D.M. Kerrick, Ed., Contact Metamorphism, 26, p. 105–206. Reviews in Mineralogy, Mineralogical Society of America, Chantilly, Virginia.
Perchuk, L.L. and Lavrent'eva, I.V. (1983) Experimental investigation of exchange equilibria in the system cordierite-garnet-biotite. In S.K. Saxena, Ed., Kinetics and Equilibrium in Mineral Reactions, 3, p. 199–239. Advances in Physical Chemistry, Springer-Verlag, New York.
Perkins, D., Holland, T.J.B., and Newton, R.C. (1981) The Al_2O_3 contents of enstatite in equilibrium with garnet in the system MgO-Al_2O_3-SiO_2 at 15–40 kbar and 900–1600 °C. Contributions to Mineralogy and Petrology, 78, 99–109.
Peterson, J.W. and Newton, R.C. (1989) Reversed experiments on biotite-quartz-feldspar melting in the system KMASH: implications for crustal anatexis. Journal of Geology, 97, 465–485.
Powell, R. and Holland, T. (1990) Calculated mineral equilibria in the pelite system, KFMASH (K_2O-FeO-MgO-Al_2O_3-SiO_2-H_2O). American Mineralogist, 75, 367–380.
Rancourt, D.G., Mercier, P.H.J., Cherniak, D.J., Desgreniers, S., Kodama, H., Robert, J.L., and Murad, E. (2001) Mechanisms and crystal chemistry of oxidation in annite; resolving the hydrogen-loss and vacancy reactions. Clays and Clay Minerals, 49, 455–491.
Rebbert, C.R., Partin, E., and Hewitt, D.A. (1995) Synthetic biotite oxidation under hydrothermal conditions. American Mineralogist, 80, 345–354.
Redhammer, G.J. and Roth, G. (2002) Single-crystal structure refinements and crystal chemistry of synthetic trioctahedral micas $KM_3(Al^{3+},Si^{4+})_4O_{10}(OH)_2$, where M = Ni^{2+}, Mg^{2+}, Co^{2+}, Fe^{2+}, or Al^{3+}. American Mineralogist, 87, 1464–1476.
Redhammer, G.J., Beran, A., Schneider, J., Amthauer, G., and Lottermoser, W. (2000) Spectroscopic and structural properties of synthetic micas on the annite-siderophyllite binary: synthesis, crystal structure refinement, Moessbauer, and infrared spectroscopy. American Mineralogist, 85, 449–465.
Robert, J.L. (1976) Phlogopite solid solutions in the system K_2O-MgO-Al_2O-SiO_2-H_2O. Chemical Geology, 17, 195–212.
Rutherford, M.J. (1973) The phase relations of aluminous iron biotites in the system $AlSi_3O_8$-$KAlSiO_4$-Al_2O_3-Fe-O-H. Journal of Petrology, 14, 159–180.
Schairer, J.F. and Bowen, N.L. (1955) The system K_2O-Al_2O_3-SiO_2. American Journal of Science, 253, 681–746.
Spear, F.S. and Cheney, J.T. (1989) A petrogenetic grid for pelitic schists in the system SiO_2-Al_2O_3-FeO-MgO-K_2O-H_2O. Contributions to Mineralogy and Petrology, 101, 149–164.
Wei, C. and Powell, R. (2003) Phase relations in high-pressure metapelites in the system KFMASH (K_2O-FeO-MgO-Al_2O_3-SiO_2-H_2O) with application to natural rocks. Contributions to Mineralogy and Petrology, 145, 301–315.
Wones, D.R. and Dodge, F.C.W. (1977) The stability of phlogopite in the presence of quartz and diopside. In D.G. Fraser, Ed., Thermodynamics in Geology, p. 229–247. Reidel, Dordrecht, Holland.
Wood, B.J. (1976) The reaction phlogopite + quartz = enstatite + sanidine + H_2O, Progress in Experimental Petrology, Natural Environment Research Council, Ser. D, 17–19.
Wood, B.J. and Nicholls, J. (1978) The thermodynamic properties of reciprocal solid solutions. Contributions to Mineralogy and Petrology, 66, 389–400.
Woodland, A.B. and Wood, B.J. (1989) Electrochemical measurement of the free energy of almandine ($Fe_3Al_2Si_3O_{12}$) garnet. Geochimica et Cosmochimica Acta, 53, 2277–2282.
Wu, C., Zhang, J., and Ren, L. (2004) Empirical garnet-biotite-plagioclase-quartz (GBPQ) geobarometry in medium- to high-grade metapelites. Journal of Petrology, 45 1907–1921.
Xu, G., Will, T.M., and Powell, R. (1994) A calculated petrogenetic grid for the system K_2O-FeO-MgO-Al_2O_3-SiO_2-H_2O, with particular reference to contact-metamorphosed pelites. Journal of Metamorphic Geology, 12, 99–119.
Zhou, F. (1994) Ti-Mg-Fe biotites: formation, substitution, and thermodynamic properties at 650 to 900 °C and 1.1 Kb with f_{O_2} defined by the CH_4-graphite buffer, 269 p. Ph.D. thesis, State University of New York, Stony Brook.

MANUSCRIPT RECEIVED AUGUST 1, 2005
MANUSCRIPT ACCEPTED JULY 29, 2006
MANUSCRIPT HANDLED BY EDWARD GHENT